Gold Bulletin (2021) 54:75–87
https://doi.org/10.1007/s13404-021-00295-4

ORIGINAL PAPER

Synthesis, characterization, and in vitro drug release properties of AuNPs/p(AETAC-co-VI)/Q nanocomposite hydrogels

Seçil Durmuş[1] · Betul Yilmaz[1] · Mehmet Rıza Kıvanç[2] · Alper Onder[3] · Pinar Ilgin[4] · Hava Ozay[5] · Ozgur Ozay[5,6]

Received: 30 December 2020 / Accepted: 7 April 2021 / Published online: 14 April 2021

Abstract

In this study, the cationic monomer [2-(acryloyloxy)ethyl]trimethylammonium chloride solution (AETAC) and vinyl imidazole (VI) were used with the free radical polymerization technique, which is a simple and rapid synthesis method, to synthesize p(AETAC-co-VI) hydrogels. To increase the density of cationic charge on the hydrogel, it underwent the protonation process with HCl. The obtained p(AETAC-co-VI)/Q hydrogel was modified with Au nanoparticles to increase bactericidal effect to obtain the AuNPs/p(AETAC-co-VI)/Q nanocomposite hydrogel. The morphology and chemical structure of the hydrogels were characterized with SEM and FTIR. Additionally, the swelling capabilities were tested in different pH media. XRD and TEM confirmed the formation of the nanocomposite hydrogel. The antibacterial activity of the hydrogels was tested against *E. coli* and *S. aureus*, and controlled release implementations were completed with sodium diclofenac (NaDc) drug. The NaDc drug release profiles of the hydrogels were researched using the Korsmeyer–Peppas model at 37 °C in different simulated buffer (pH 6.0, 7.2, and 8.0) solutions. It was found that both the hydrogel and nanocomposite hydrogel followed non-Fickian diffusion mechanisms as free release mechanism. Here, the maximum drug release efficacy was found to be 97%, and drug release was more rapid in basic media when release media were compared. The AuNPs/p(AETAC-co-VI)/Q nanocomposite hydrogels produced in this study with advanced antibacterial features were suitable for recommendation as good carriers for in vitro release of NaDc drugs in areas like the biomedical and pharmaceutical industries.

Keywords Hydrogel · Drug delivery · Gold nanoparticles · Wound dressing · Antimicrobial

✉ Pinar Ilgin
pinarilgin@comu.edu.tr; pinarilgin2014@gmail.com

[1] Department of Bioengineering and Materials Engineering, School of Graduate Studies, Canakkale Onsekiz Mart University, Canakkale, Turkey

[2] Vocational School of Health Services, Van Yüzüncü Yıl University, Van, Turkey

[3] Department of Chemistry, School of Graduate Studies, Canakkale Onsekiz Mart University, Canakkale, Turkey

[4] Department of Chemistry and Chemical Processing Technologies, Lapseki Vocational School, Canakkale Onsekiz Mart University, Canakkale, Lapseki, Turkey

[5] Department of Chemistry, Faculty of Science and Arts, Laboratory of Inorganic Materials, Canakkale Onsekiz Mart University, Canakkale, Turkey

[6] Department of Bioengineering, Faculty of Engineering, Canakkale Onsekiz Mart University, Canakkale, Turkey

Introduction

Hydrogels are three-dimensional polymeric networks containing crosslinks. These hydrogels are highly porous and flexible structures. They may trap high amounts of water/biological fluids within their structure and provide a structure mimicking natural tissue. Hydrogels are frequently and commonly used in the biomedical field as biosensors, for controlled drug release systems, tissue engineering, and wound cover studies [1–3]. To ensure effective and correct wound healing, there is a need to develop new-generation wound covers which release drugs. The ideal wound cover material should keep the wound moist. Additionally, it should protect the wound from external mechanical effects and pathogenic vectors. It should also have biocompatible, nontoxic properties [4, 5]. In recent times, hydrogels have been commonly used as antimicrobial polymeric material for wound healing and to prevent scars [6, 7]. During the wound healing process, hydrogels

assist in removing infectious fluid from the wound, do not cause infection, provide a suitable environment for tissue regeneration and a moist environment for the wound site, and were seen to function as ideal wound coverings [4, 8]. In spite of all the advantageous features provided by hydrogels, hydrogel-based materials may cause microbial infections in the wound site due to the moist environment. As a result, the main focus of wound bandages is to provide a moist and sterile environment for a longer time at the wound site. In recent times, a variety of studies developed many polymeric materials with antimicrobial activity to apply as wound dressings [9–11]. Cationic polymers carrying quaternized nitrogen atoms are one of these [12, 13]. Cationic-based polymers display antibacterial and anti-inflammatory effects during wound healing processes when used as dressings and treatments. They have begun to be frequently used as wound cover materials in recent times as they are biologically adhesive and biocompatible and ensure more rapid healing of the wound [14–16]. Due to concerns related to the development of microorganism resistance to antibiotics used to provide sterility at the wound site, along with polymers and hydrogels, nanoparticles have begun to be commonly used as a wound covering material with the implementation of nanotechnology to speed up the healing process [17, 18].

Gold has been mined from ancient times to the present and was one of the first metals used for medical purposes for the treatment of a variety of diseases like syphilis, leprosy, plague, epilepsy, and diarrhea [19, 20]. It is also extensively used in materials science as an effective catalyst for many reactions [21, 22]. Gold nanoparticles are chemically inert structures with easy and adjustable synthesis and extraordinary advantages like stability, high distribution, nontoxic features, and higher biological biocompatibility which has led to increasing interest in the use of gold nanoparticles (AuNP) in recent times [23, 24]. Gold has both bacteriostatic and bactericidal activities and so is used as an antimicrobial agent [25–27]. In addition to antimicrobial activity, gold nanoparticles accelerate the healing process and encourage wound healing [28]. The inclusion of Au nanoparticles, an increasing trend at present, within multifunctional polymeric networks especially is a promising implementation with a broad range of biomedical applications such as biosensor [29], biomedical imaging [30, 31], antimicrobial applications [32], and targeted drug delivery [33, 34].

Both cationic polymers and AuNPs have antimicrobial potential, so a composite structure created using both materials may assist in the development of microbial performance. These nanoparticles ensure maximization of strong bonds with the drug molecules in the polymer, drug release efficacy in the desired area, lowest side effects, and lower dosing frequency.

As a result, in this study, hydrogels were synthesized by the free radical polymerization technique, which is a simple and fast synthesis method, using cationic monomer of [2-(acryloyloxy)ethyl] trimethylammonium chloride solution (AETAC) and neutral monomer of vinyl imidazole (VI). Due to the possibility that the surfaces of the synthesized hydrogels may display toxic or antiallergic effects, they were modified with the Au nanoparticles as an antimicrobial agent in order to make them suitable as a wound cover. We designed a wound cover material with controlled drug release system showing antibacterial features. In this way, the efficacy of wound treatments and dressings will be an increased providing accelerated wound healing. The aim of this study is to observe the sustainable drug release and antimicrobial efficacy of the AuNPs/p(AETAC-co-VI)/Q hydrogel, considered to be an alternative wound cover, for sodium diclofenac (NaDc) model drug. The release of NaDc drug from the nanocomposite p(AETAC-co-VI)/Q hydrogels with the contribution of Au nanoparticles is new in the literature. The present study is expected to provide an ideal method for the synthesis of hydrogels with sufficient antimicrobial potential for controlled release of diclofenac.

Experimental

Materials

For the polymer synthesis, [2-(acryloyloxy)ethyl]trimethylammonium chloride solution (AETAC, 80 wt.% in H_2O), 1-vinylimidazole (VI, 99%), ammonium persulfate (APS, 99.9%), N,N,N′,N′-tetramethylethylenediamine (TEMED, 99%), and N,N′-methylenebisacrylamide (MBA, 99%) were purchased from Sigma-Aldrich. For the AuNP preparation, potassium gold (III) chloride (99.9%) was purchased from Sigma-Aldrich, and trisodium citrate (99%) was received from Isolab chemicals. For the drug loading and release studies, sodium diclofenac (NaDc, 98%) was purchased as a model drug from Acros. For the antimicrobial studies, tryptic soy agar (TSA) and tryptic soy broth (TSB) were purchased from Merck. All chemicals were used without further purification. Distilled water (DW) was used in all stages of the experimental studies.

Swelling and drug release studies were determined in pH 6.0 buffer (phosphate buffer, PB), pH 7.2 buffer (phosphate buffer saline, PBS), and pH 8.0 buffer (simulated wound fluid, SWF). The pH 6.0 buffer was prepared with 0.1 M KH_2PO_4 in 100 mL of DW. PBS was prepared by mixing 0.806 g of NaCl, 0.027 g of KH_2PO_4, 0.178 g of $Na_2HPO_4{\cdot}H_2O$, and 0.020 g of KCl in a volumetric flask to reach a volume of 100 mL with DW. SWF was prepared by taking 0.68 g of NaCl, 0.22 g of KCl, 2.5 g of $NaHCO_3$, and 0.35 g of NaH_2PO_4 in 100 mL of DW. The pH of all solutions were adjusted with 0.1 M NaOH [35, 36].

Preparation of hydrogels

Firstly, similar to our previous studies, cationic-based hydrogels with various feed components were synthesized with the free radical copolymerization technique [37, 38]. For this, the neutral monomer of VI and the cationic monomer of AETAC were used. Hydrogels contained 3 different molar ratios of AETAC and VI monomers of 1:1, 2:1, and 1:2. As crosslinker, 1% MBA (of total monomer ratio) was weighed and dissolved in 500 μl distilled water. The molar ratios of AETAC and VI monomers given in Table 1 were dissolved in each other, and the crosslinker was added to this solution. The obtained homogeneous solution had 500 μl 1% APS (of total monomer ratio) and 50 μl TEMED added to begin the reaction. Polymerization of the prepared solution was completed in straws with an internal diameter of 5 mm. After gelation is completed, the cylindrical gels were cut to 5 mm size. The synthesized p(AETAC-co-VI) hydrogels were washed with distilled water 3 times during 1 day and then dried in an oven at 40 °C for 24 h. The yield of the obtained hydrogels was calculated according to Eq. 1 [39]. The dried gels were quaternized and called p(AETAC-co-VI)/Q. The quaternization procedure was completed by leaving the hydrogels in 2% hydrochloric acid (HCl) aqueous solution for 24 h. After the quaternization procedure, the quaternized hydrogels were washed with distilled water to remove excess acid and dried again in an oven.

Later, 40 mg of quaternized hydrogels prepared at 1:1 ratio of AETAC to VI were left for 1 day in potassium gold (III) chloride solution (1.45 mM, 40 ml) in a dark environment. After this procedure, the hydrogels were reduced with trisodium citrate (10 mM, 40 mL), washed again with distilled water, and dried in an oven. The gold-loaded hydrogels were named AuNPs/p(AETAC-co-VI)/Q:

$$\text{Yield}\% = \frac{W_c}{W_i} x100 \quad (1)$$

where W_i is the total weight of the monomers (VI, AETAC, and MBA) and W_c is the dry weight after synthesis.

Swelling studies of hydrogels

The swelling behavior of the hydrogels in distilled water or buffer solution was investigated. Equilibrium swelling rates were investigated with the gravimetric method. Firstly, dry hydrogel with a known initial mass (M_i) was dipped in a swelling solution at room temperature, and the mass was measured at certain time intervals (M_t) until equilibrium swelling was reached. During measurements, the hydrogel was removed from water, and excess water on the hydrogel surface was removed with filter paper. The swelling ratio (SR) at equilibrium was determined using the following equation [40]:

$$SR\% = (M_t - M_i)/M_i x100 \quad (2)$$

Drug loading and release from hydrogels

Dry p(AETAC-co-VI)/Q(1:1) hydrogel and AuNPs/p(AETAC-co-VI)/Q(1:1), each weighing 0.1 g, were transferred to 100-mL diclofenac sodium aqueous solution (50 mg/L). They were stored at room temperature for 2 days to ensure the hydrogel reached equilibrium drug loading status. Before loading, the drug concentration within the supernatant was measured at 276 nm with UV-Vis spectroscopy (T80+ UV/VIS Spectrometer, PG Ins. Ltd.), and the loading amount was calculated using Eq. 3 [41]. The drug-loaded hydrogels were dried at room temperature. For in vitro release studies, 0.1 g dry gels were placed in 25 mL of different buffer pH solutions at 37 °C, and release amount was measured until release equilibrium was reached. The release amount was calculated using Eq. 4 [40]. The response to pH variations was examined by using pH 6.0 (PB), pH 7.2 (PBS), and pH 8.0 (SWF) buffer solutions as release media.

$$q_e = (C_i - C_e) * V/M \quad (3)$$

Table 1 The synthesis compositions and diffusion parameters of hydrogels

Hydrogels	AETAC (mmol)	VI (mmol)	SR%	Yield %	n	k_p	Diffusion type
p(AETAC-co-VI)(1:1)	5	5	842	75.3	0.62	0.046	Non-Fickian
p(AETAC-co-VI)/Q(1:1)	5	5	993	-	0.53	0.063	Non-Fickian
p(AETAC-co-VI) (2:1)	6.6	3.3	1110	76.9	0.59	0.050	Non-Fickian
p(AETAC-co-VI)/Q(2:1)	6.6	3.3	1350	-	0.74	0.042	Non-Fickian
p(AETAC-co-VI) (1:2)	3.3	6.6	1032	72.1	0.58	0.026	Non-Fickian
p(AETAC-co-VI)/Q(1:2)	3.3	6.6	1285	-	0.49	0.088	Non-Fickian

-, non-calculated

$$\text{Drug release percent}\ (\%) = \frac{\text{Released drug from hydrogel}}{\text{Total drug in the hydrogel}} x100 \quad (4)$$

where C_i and C_e are the concentrations of drug solution at the initial time and equilibrium time, respectively, V is the volume of the drug solution (L), and M is the amount of the dry hydrogel (g).

Korsmeyer–Peppas model for swelling and drug release studies

Diffusion mechanisms for swelling and drug release from the polymer matrix were evaluated using the Korsmeyer and Peppas equation, Eq. 5:

$$log\frac{M_t}{M_\infty} = logk_p + nlogt \quad (5)$$

where M_t is the swelling/drug release at time t, M_∞ is the swelling/drug release at equilibrium, k_p is the gel characteristic constant, and n is the diffusion exponent describing the swelling or release mechanism. The plots of log M_t/M_∞, versus log t were plotted using 60% of the experimental data. Values of n and k were calculated from the slopes and intercepts of these plots. A value of $n = 0.45$ indicates Fickian diffusion mechanism; $0.45 < n < 0.89$ indicates non-Fickian diffusion (combination of diffusion and relaxation); $n = 0.89$ indicates a case 2 transport (relaxation-controlled), and $n > 0.89$ is super case 2 transport [41, 42].

Antimicrobial studies

Escherichia coli (*E. coli*) (gram-negative) ATCC 8739 and *Staphylococcus aureus* (*S. Aureus*) (gram-positive) ATCC 6538 bacteria were used for the disk diffusion test. To obtain overnight culture, initially colonies were suspended in 15-mL TSB medium and mixed at 100 rpm overnight at 37 °C. Later 50-µl bacterial suspension was spread in one direction on the petri dishes prepared with TSA using a sterile rod. Later, all swollen hydrogel disks with 8.0 mm diameter and 3.0 mm thickness were placed on the surface of medium inoculated with bacteria. The petri dishes were incubated overnight at 37 °C, and the diameter of inhibition regions was measured (including the area covered by hydrogel) with the aid of a ruler.

Characterization

The surface morphology of p(AETAC-co-VI)/Q(1:1) hydrogel was researched with a scanning electron microscope (SEM) JEOL 7100-EDX device. A thin section was obtained from the swollen hydrogen, and trapped water was removed with a lyophilizer while preserving the porous structure. Samples were coated in Au/Pd to 80:20 ratio before measurements.

Fourier transform infrared (FTIR) analysis with ATR apparatus was used to determine the characteristic functional groups and chemical structure of the hydrogel and monomer samples at 650–4000 cm^{-1} wavelength (4 cm^{-1} resolution) with an FTIR spectrometer ((Perkin Elmer 100 spectrometer).

A Perkin Elmer TGA 8000 device was used in order to determine the thermal properties of the p(AETAC-co-VI)/Q(1:1) hydrogel. Analysis conditions used the interval 30 to 900 °C, nitrogen gas flow, and 10 °C/min heating rate.

X-ray diffraction (XRD) analyses were completed in order to determine the crystallinity of the p(AETAC-co-VI)/Q(1:1) hydrogel and AuNPs/p(AETAC-co-VI)/Q(1:1) nanocomposite hydrogel and to analyze AuNPs within the hydrogel. Using a PANalytical Empyrean device, operating parameters were λ = 1.54056 Å at 45 kV and 40 mA.

A transmission electron microscope (TEM, Hitachi High-Tech HT7700) was used in order to determine the dimensions of AuNPs within the AuNPs/p(AETAC-co-VI)/Q(1:1) nanocomposite hydrogel and to take micrographs of the AuNP particles.

Results and discussion

P(AETAC-co-VI)-derived hydrogels were synthesized by free radical cross-linked copolymerization in an aqueous solution using AETAC cationic monomer, VI neutral monomer, MBA crosslinker, and APS redox initiator. The estimated synthesis reaction for the hydrogel is shown in Fig. 1a. The comonomer ratios used for the new hydrogels were changed during synthesis, and the feed content for all monomers and synthesis compounds are given in Table 1. All polymers were obtained in a cylindrical form and the macroscopic structure was preserved after removing unreacted compounds. The dry sample of p(AETAC-co-VI) hydrogel is a cationic structure due to the AETAC monomer in the structure; however, when contacted with an acid solution, imidazole ring groups may be protonated as the imidazole ring groups on p(AETAC-co-VI) hydrogel are basic ($Im + H^+ = ImH^+$) [38]. Thus, increases were provided in the positive charge density of the hydrogels. This reaction is shown in Fig. 1b.

The FTIR spectrum of AETAC monomer, VI monomer, p(AETAC-co-VI) hydrogel, and quaternized p(AETAC-co-VI)(1:1) are shown in Fig. 2. The main peaks of AETAC groups in the hydrogel spectrum are assigned to the C=O of ester group at 1730 cm^{-1}, C–N stretching vibration at 951 cm^{-1} of quaternary ammonium groups, and symmetric and asymmetric stretching vibrations of C–H of the methylene groups at 2938 and 3029 cm^{-1} [37]. In addition to the above bands, the main peaks of VI groups in the hydrogel spectrum

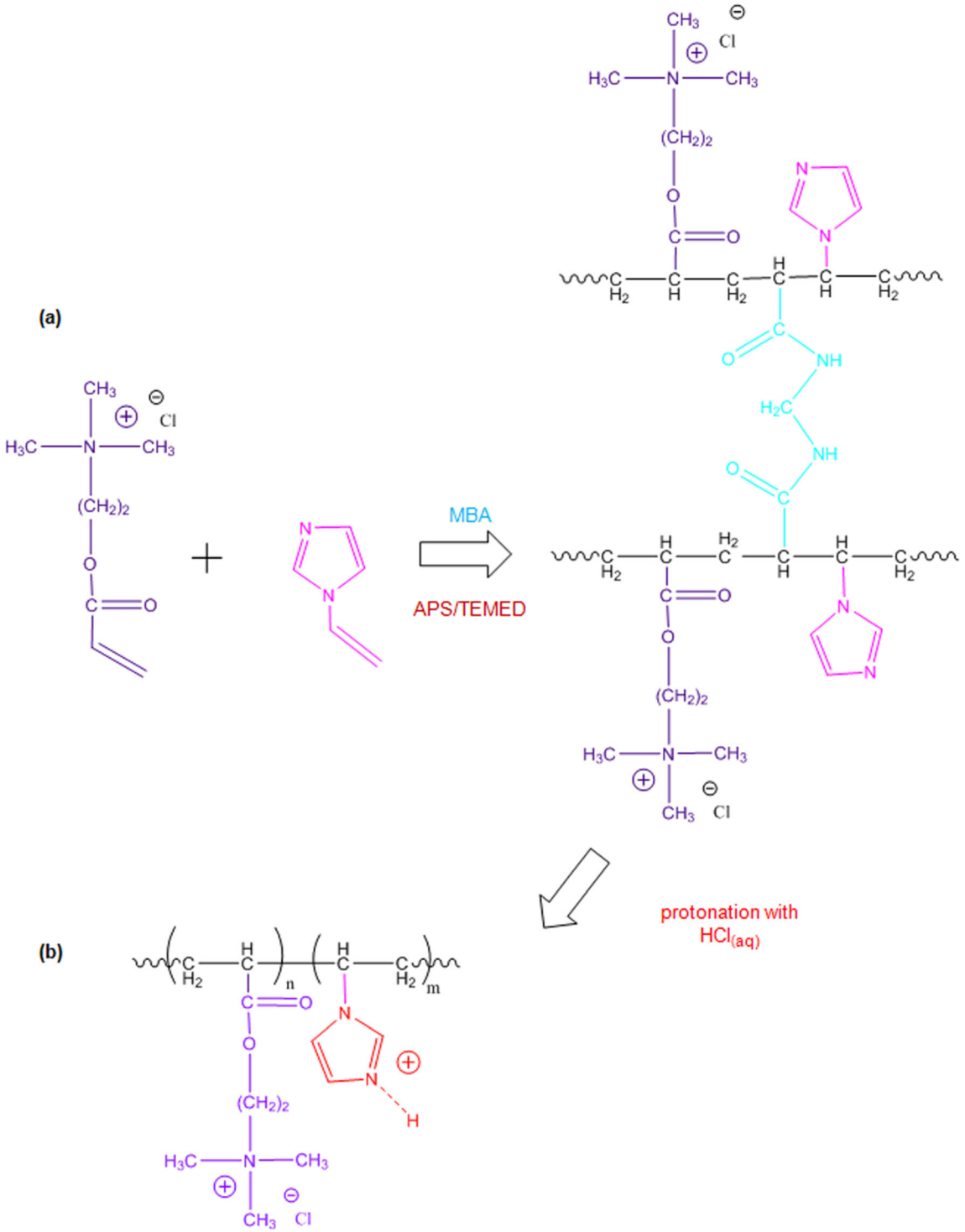

Fig. 1 Schematic synthesis mechanism of **a** p(AETAC-co-VI) hydrogel and **b** p(AETAC-co-VI)/Q hydrogel

are assigned to the C=C ring stretching at 1645 cm^{-1}, C=N ring stretching at 1487 cm^{-1}, and C–H ring stretching at 3100 cm^{-1} [43]. Additionally, the characteristic absorption bands observed at 1645 and 1583 cm^{-1} correspond to the stretching of amide groups in MBA in the hydrogels. These results show that the hydrogels were successfully created by copolymerization of AETAC, VI, and MBA compounds.

To prove the quaternization of p(AETAC-co-VI)(1:1) hydrogel, the FTIR spectra in Fig. 2d for p(AETAC-co-VI)(1:1) and p(AETAC-co-VI)/Q(1:1) were compared. While new adsorption bands occurred, some bands were lost or weakened. The adsorption band at 1085 cm^{-1} flattened, and a new absorption band obtained at 1542 cm^{-1} was assigned to the vibration mode of the $–N^{+}–H$ structure produced during the

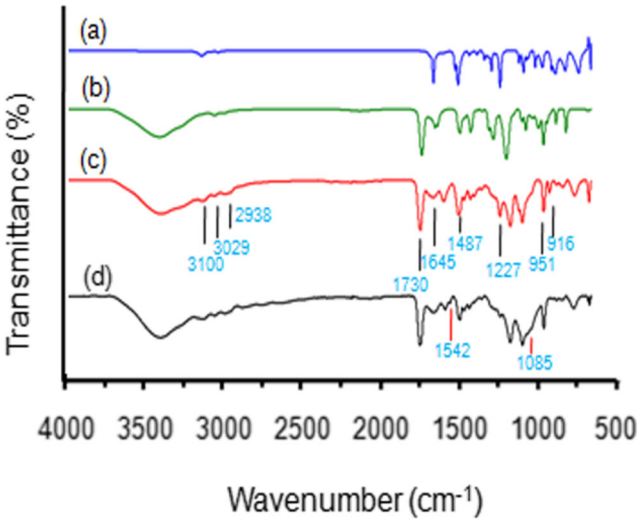

Fig. 2 FTIR spectrum of the **a** VI monomer, **b** AETAC monomer, **c** p(AETAC-co-VI) hydrogel, and **d** p(AETAC-co-VI)/Q hydrogel

protonation process confirming the quaternized imidazole ring. After the quaternization procedure, the sharp absorption bands equivalent to C–N stretching of the imidazole ring at 1227 and 916 cm^{v1} were very much reduced. These changes show successful quaternization of the N atom on the imidazole ring [44].

The water absorption or water absorption rate of a hydrogel polymer is linked to the network porosity of the hydrogel. As a result, it is important to assess the microstructure of the hydrogen morphologically. Network structure morphology of the p(AETAC-co-VI)/Q(1:1) hydrogel was examined with SEM. A thin disk was cut from the swollen hydrogel and frozen to −80 °C and then lyophilized to remove water from the network structure. Thus, the porous structure of the hydrogel was preserved. Images of SEM micrographs of the hydrogel are shown in Fig. 3. The figure clearly shows the cross-linked and very porous internal structure of the hydrogel. Most pores are created by linked channels. Additionally, the porous structure contains well-defined macropores with 0.2–12 μm size. These pores may be said to be effective water-permeable regions for drug release applications [34, 39].

The TGA-DTA thermograms for p(AETAC-co-VI)/Q(1:1) are presented in Fig. 4. Changes in the thermal properties of the hydrogel were researched using a thermogravimetric analyzer from 30 to 900 °C under nitrogen atmosphere. The hydrogel showed degradation behavior in 4 main stages. In the first stage, 11.3% weight loss occurred from 30 to 220 °C, and water remaining in the structure was removed. The second stage with rapid and large mass reduction due to breaking of the polymer chains was identified between 238 and 377 °C. The main degradation of the synthesized hydrogel may be linked to depolymerization of the network structure by breaking of C–C bonds and degradation of the cross-linked polymeric structure. The hydrogel lost 55.2% of weight in this degradation. The third stage was identified from 377 to 490 °C and 10.1% weight loss occurred. The final stage was identified between 490 and 900 °C, and 21.2% weight loss occurred. The final two degradation stages may be attributed to a complicated process dominated by the degradation of AETAC and VI/Q structures. During degradation up to 900 °C, 97.7% of the total mass was lost. All four steps are consistent with the main peaks of the DTG curves. From the DTA curves, an endothermic peak point was identified as equivalent to 318 °C with depolymerization causing main mass loss. It was concluded that the inclusion of monomers in the network structure resulted in the formation of a thermally stable hydrogel from the above results.

Hydrogels have the ability to swell by absorbing water or biological fluids with the aid of a variety of functional groups found in the network structure. This swelling behavior is an important property that determines the applications for hydrogel material. Absorption and holding of wound fluids are necessary for wound debridement and preservation of moist wound environment for better wound healing. Figure 5a shows the equilibrium water contents for distilled water at 20 °C for hydrogels with a variety of feed monomer contents. As the monomer feed content increased, the swelling behavior increased due to the development of additional osmotic pressure in the expanding gel network. Accordingly, swelling percentages according to feed content of p(AETAC-co-VI) hydrogels were 1110 for 2:1, 1032 for 1:2 and 842 for 1:1 at the end of 420 min. After protonation of the hydrogels, the

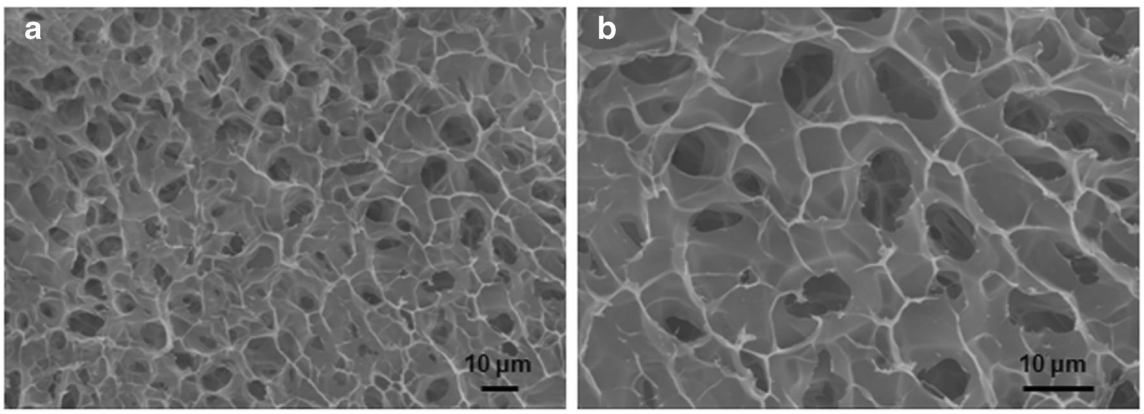

Fig. 3 SEM images of the p(AETAC-co-VI)/Q hydrogel for different magnifications **a** ×750 and **b** ×1500

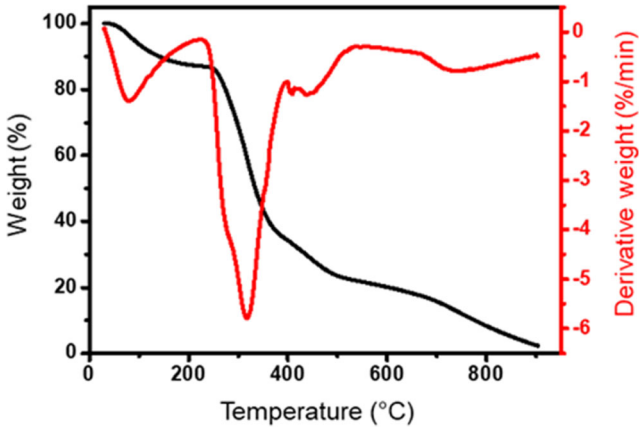

Fig. 4 TGA curve of the p(AETAC-co-VI)/Q hydrogel

positive charge intensity of the network structure increased due to easy protonation of amino groups. Thus, the swelling behavior of quaternized hydrogels increased. The reason for this is that positive charges in the network structure repel each other, so the network structure expands, and more water can penetrate the network structure [45]. Accordingly, the swelling percentages for p(AETAC-co-VI)/Q(1:1) hydrogels according to feed content were 1350 for 2:1, 1285 for 1:2, and 993 for 1:1 at the end of 420 min.

The swelling behavior of p(AETAC-co-VI)/Q(1:1) hydrogels was examined at 20 °C in distilled water, pH 6.0 (PB), pH 7.2 (PBS), and pH 8.0 (SWF) buffer solution media, and Fig. 5b shows the equilibrium fluid content according to time at 20 °C. Hydrogels had maximum osmotic pressure in distilled water which ensured the gel easily absorbed water from the medium and held it at high rates. In pH 6.0 (PB), pH 7.2 (PBS), and pH 8.0 (SWF) buffer solution media, the percentage swelling values for hydrogels were as follows: 799, 655, and 594, respectively. Here, the swelling rates of hydrogels were reduced compared to distilled water. Swelling of hydrogels was affected by the pH of the swelling medium. In the situation with simulated wound fluid (pH 8.0), the percentage swelling ratio was observed to reduce compared to pH 6.0 buffer. The reason for this may be due to the protonated VI groups within the hydrogel network structure being deprotonated as the medium pH increased, causing a reduction in ionic repulsion between functional sections. Additionally, the presence of a variety of ions in the pH 6.0 (PB), pH 7.2 (PBS), and pH 8.0 (SWF) buffer solution media may have increased ionic power of the medium causing a reduction in osmotic pressure difference between the network structure and surrounding solution [46]. In conclusion, there is compatibility between swelling values at different pH values. Hydrogels may be designed according to application because wound pH may vary with the time and stage of wound healing.

In Fig. 5a and b, the Korsmeyer–Peppas model was applied to swelling tests in order to determine the control mechanism for the swelling process of the hydrogel and the nature of

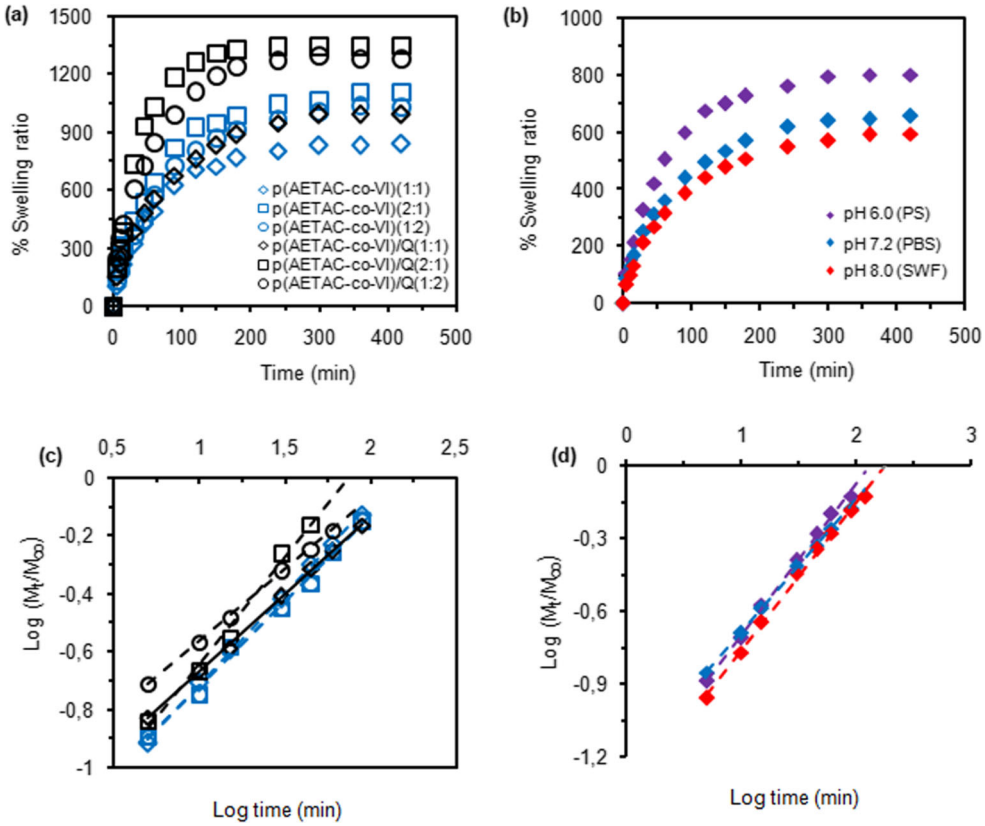

Fig. 5 Comparative swelling curve of **a** p(AETAC-co-VI) hydrogels with different feed ratios in distilled water and **b** p(AETAC-co-VI)/Q(1:1) hydrogels in various pH buffer solution. Swelling kinetics curves of **c** p(AETAC-co-VI) hydrogels with different feed ratios in distilled water and **d** p(AETAC-co-VI)/Q hydrogels in various pH buffer solution

Table 2 The diffusion parameters of p(AETAC-co-VI)/Q(1:1) hydrogels in buffer solutions

Swelling media	n	k_p	Diffusion type
pH 6.0	0.547	0.058	Non-Fickian
pH 7.2	0.609	0.043	Non-Fickian
pH 8.0	0.624	0.048	Non-Fickian

diffusion of liquid into the gel. This study is also a beneficial preliminary test for determining the diffusion of a drug from the distribution media into the hydrogel. When the dry hydrogel is contacted with an aqueous medium, firstly water molecules spread into the polymer network, and the polymer chain begins to loosen. Thus, the polymer network expands towards the medium and swelling occurs. The parameter values calculated from the slope and intersection points on the graphs in Fig. 5c and d are listed in Table 2. There were perfect correlation coefficients for all media. As can be seen from Table 2, the n values were between 0.45 and 0.89 at 20 °C for swelling studies in all three media. From these results, the swelling mechanism in all media was dominantly non-Fickian diffusion. Accordingly, the penetration mechanism for water is diffusion and is controlled by loosening of the polymer chain [47]. Hydrogels containing gold nanoparticles have become an active research area due to their amazing potential in a variety of applications. In this study, with the aim of increasing the antibacterial efficacy of the obtained hydrogels, gold nanoparticles (AuNPs) were included in the hydrogels. The negative-charge gold nanoparticles ($AuCl_4^-$) require positive charge on the hydrogel particle surfaces to bind to the surface. It is necessary to discuss the important role of VI in this study. The imidazole ring may be protonated as a result of treatment with acid. Thus, the positive charge density on the hydrogel surface is increased. The p(AETAC-co-VI)/Q hydrogels may attract the negative-charge $AuCl_4^-$ ions via electrostatic interactions with the quaternized ammonium ($-N^+$) groups [48]. In practice, the hydrogel was dipped in a Au^{3+} solution in a dark environment for 24 h; thus, diffusion of the gold solution was ensured into the pores in the hydrogel network. Later, the Au^{3+} ions were reduced to AuNP using sodium citrate. This reduction reaction caused a color change showing the production of Au nanoparticles, and the yellow-colored hydrogel turned brown. In this way, an alternative green strategy provides advantages for the production of AuNPs without creating probable toxic by-products [49]. Figure 6 shows the production of gold nanocomposite hydrogels. Networks around the gold nanocomposite hydrogel may effectively absorb drugs containing nitrogen and oxygen and later release the absorbed drug in the required release environment [50].

The natures of the p(AETAC-co-VI)/Q hydrogel and AuNPs/p(AETAC-co-VI)/Q nanocomposite hydrogel were determined with X-ray diffraction as in Fig. 7. The X-ray diffraction pattern of the p(AETAC-co-VI)/Q hydrogel shows a broad XRD peak at 2θ around 23.25°. This may be due to the amorphous nature of the crystal forms in the hydrogel. However, the semi-crystalline peak density of the p(AETAC-co-VI)/Q reduces with an increase in the broadness of the peak after the addition of gold nanoparticles to the hydrogel. This is linked to the interaction of gold nanoparticles with the p(AETAC-co-VI)/Q hydrogels. The Bragg reflection patterns of 2θ = 38.38° (111), 44.47° (200), and 64.81° (220) confirm the face central cubic (FCC) geometry of the gold nanoparticles (JCPDS NO, 4–0784) [20, 51]. Thus, the results revealed that gold nanoparticles were successfully synthesized within the polymeric structure of the p(AETAC-co-VI)/Q hydrogel. The synthesized gold nanoparticles increase the anisotropy of the material and cause a more crystalline form [20]. These results are consistent with previous studies [52, 53].

TEM analysis was completed to confirm the successful synthesis of gold nanoparticles within the hydrogel network structure. Figure 8 shows the appearance of gold nanoparticles synthesized within the p(AETAC-co-VI)/Q hydrogel. The TEM images of the AuNP/p(AETAC-co-VI)/Q nanocomposite show that the spherical-shaped gold nanoparticles with a mean diameter 7.06 ± 1.76 nm were successfully synthesized within the hydrogel network structure. Most have a spherical shape, with narrow size distribution, and uniform distribution in the suspension medium.

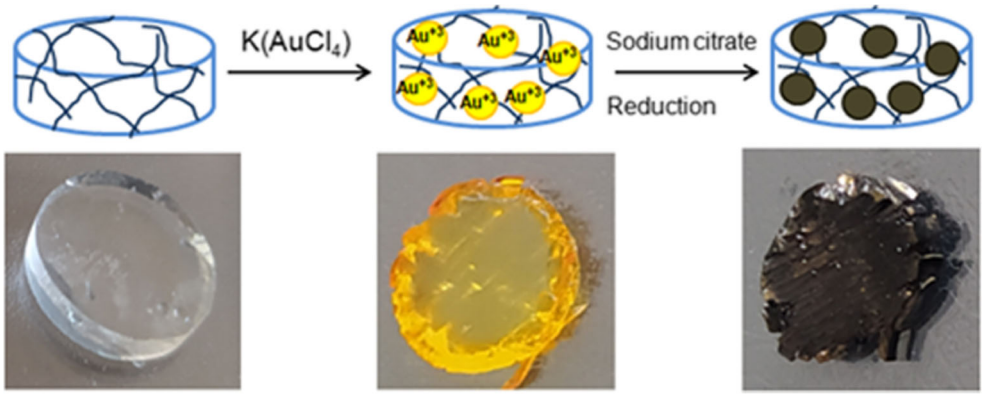

Fig. 6 Schematic diagram for the formation of AuNPs/p(AETAC-co-VI)/Q nanocomposite hydrogels

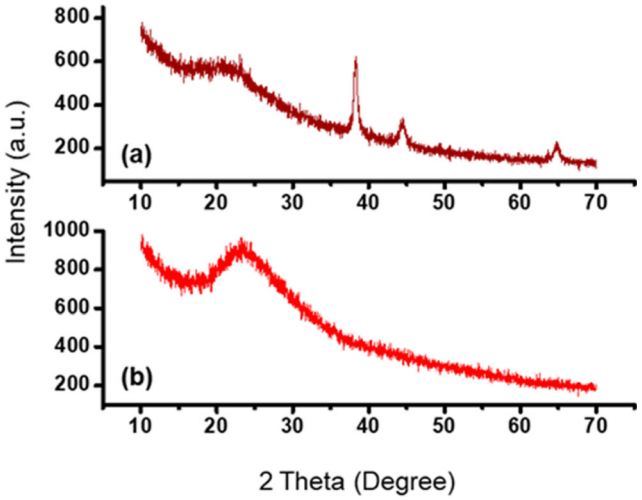

Fig. 7 XRD spectra of **a** AuNPs/p(AETAC-co-VI)/Q nanocomposite hydrogel and **b** p(AETAC-co-VI)/Q hydrogel

Gold nanoparticles are accepted as a nontoxic, environmentally friendly antibacterial material. Recent developments targeted the discovery of promising materials displaying antimicrobial activity by the inclusion of antimicrobial agents like AuNP within polymeric gel networks for biomedical applications like skin infection treatment, coatings for medical implants, and wound healing [49, 52]. The disk diffusion test was used to research the antibacterial activity of p(AETAC-co-VI) hydrogel derivatives on *E. coli* and *S. aureus*. After overnight incubation at 37 °C, each of the samples was observed to have an inhibition region. Figure 9 shows the results of the disk diffusion experiments for *E. coli* and *S. aureus*. The unprotonated partially positively charged hydrogels only showed inhibition within the area of their own diameter (8 mm) concluding that the hydrogels have no harmful effect. The open inhibition region around the hydrogel disks containing AuNP shows increasingly enhanced antibacterial activity. For these hydrogels, the inhibition region for *S. aureus* was 18 mm, while it was 11 mm for *E. coli*. As can be seen from the dimensions of the inhibition regions, the addition of AuNP significantly developed antibacterial capabilities compared to the antibacterial effect of hydrogels not containing gold. Based on the obtained bacterial inhibition data, the p(AETAC-co-VI) hydrogel containing AuNP may be said to offer valuable new opportunities for wound infection treatment.

To observe the controlled release effect for the model drug NaDc from gold nanoparticles within the polymer network, both p(AETAC-co-VI)/Q (without AuNP) hydrogel and AuNPs/p(AETAC-co-VI)/Q nanocomposite hydrogel were used as drug carriers. The drug loading amounts in the p(AETAC-co-VI)/Q and AuNPs/p(AETAC-co-VI)/Q hydrogels were 21.2 mg/g and 26.6 mg/g, respectively. As shown in Fig. 10a and b, higher amounts of drug were loaded into the AuNPs/p(AETAC-co-VI)/Q nanocomposite hydrogel compared to the p(AETAC-co-VI)/Q hydrogel. The reason for this increase may be attributed to the free adsorption regions within the network having strong affinity for NaDc molecules, allowing more diffusion of drug molecules. In addition to AuNPs/p(AETAC-co-VI)/Q nanocomposite hydrogel containing quaternized amine groups, it contains carboxylate groups and -NH groups acting as binders for NaDc among interaction regions for AuNPs. As a result, NaDc drug enters

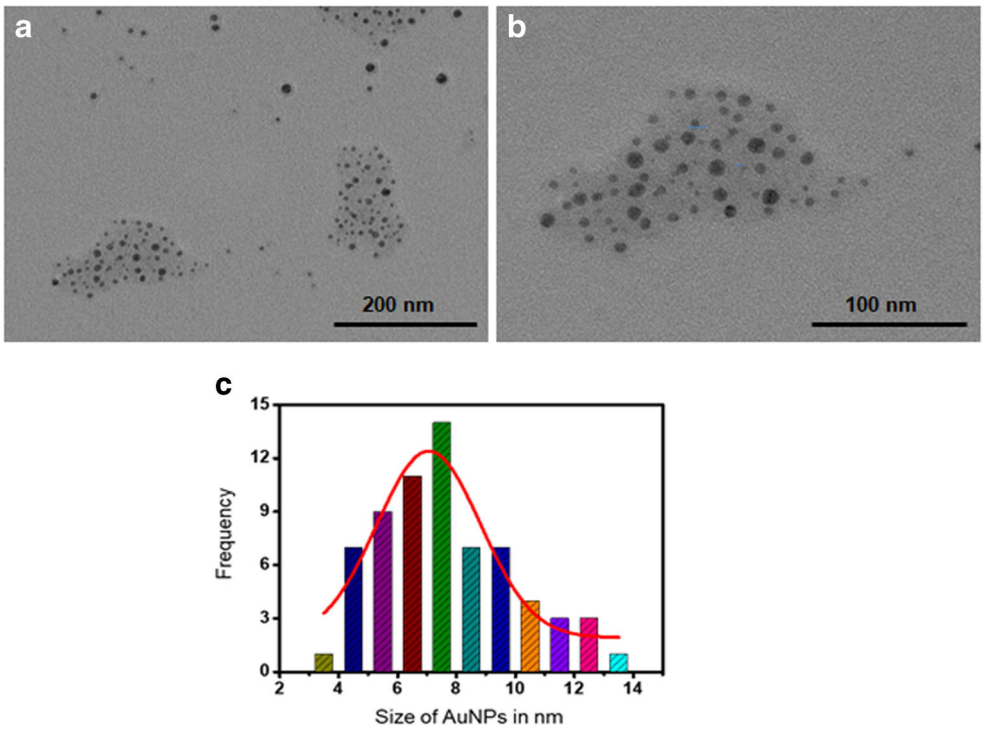

Fig. 8 **a** and **b** TEM images of the AuNPs/p(AETAC-co-VI)/Q nanocomposite hydrogel and **c** particle size distribution of synthesized AuNP nanoparticle in hydrogel

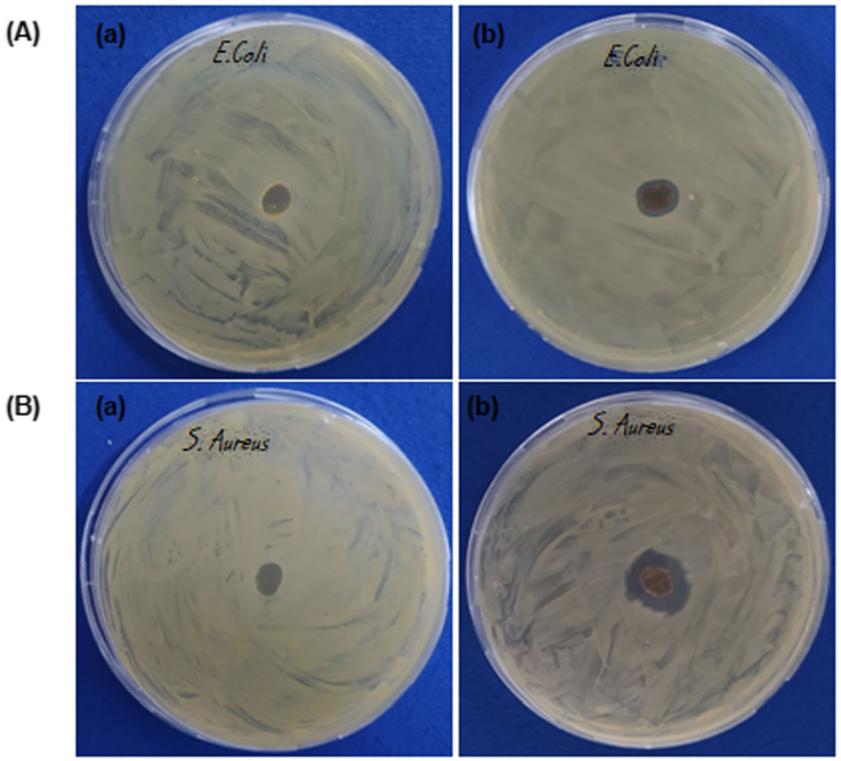

Fig. 9 Antimicrobial activity test of **a** p(AETAC-co-VI) hydrogel and **b** AuNPs/p(AETAC-co-VI)/Q nanocomposite hydrogel against (**A**) *E. coli* and (**B**) *S. aureus*

interaction with AuNP-hydrogels through physical binding like hydrogen bonds/electrostatic interactions. Release tests from the hydrogel samples loaded with NaDc identified the percentage drug content was a function of time with drug release completed at 37 °C in a variety of media with different pH values (pH 6.0 (PB), pH 7.2 (PBS), pH 8.0 (SWF) buffer

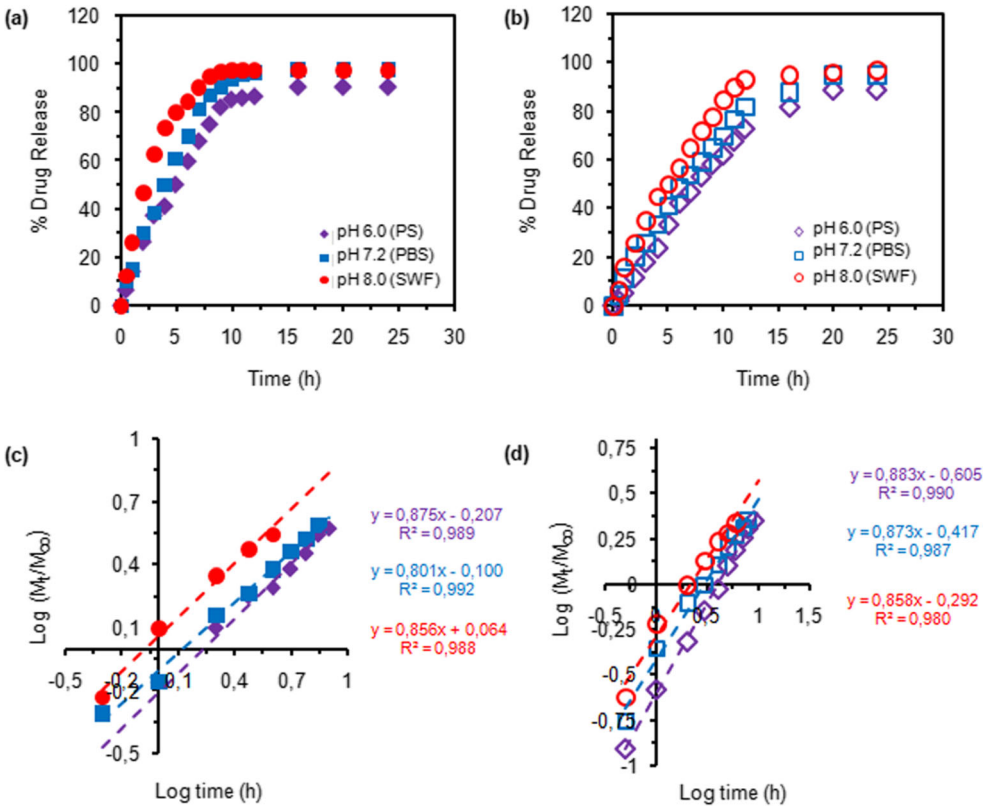

Fig. 10 NaDc delivery using **a** p(AETAC-co-VI)/Q(1:1) hydrogel and **b** AuNPs/p(AETAC-co-VI)/Q nanocomposite hydrogel as drugs carrier; drug release Korsmeyer–Peppas plots **c** p(AETAC-co-VI)/Q and **d** AuNPs/p(AETAC-co-VI)/Q

Table 3 Diffusion parameters of hydrogels in buffer solutions

Releasing media	p(AETAC-co-VI)(1:1)		p(AETAC-co-VI)/Q(1:1)		
	n	k_p	n	k_p	Diffusion type
pH 6.0	0.87	0.62	0.88	0.25	Non-Fickian
pH 7.2	0.80	0.79	0.87	0.38	Non-Fickian
pH 8.0	0.85	0.86	0.85	0.51	Non-Fickian

solutions). The effect of pH on the controlled release of NaDc using AuNPs/p(AETAC-co-VI)/Q and p(AETAC-co-VI)/Q hydrogels is presented in Fig. 10. It is clear that the absorbed ratio dramatically increased at the start of the test and later reduced in steps to reach a final plateau. As seen in the figure, the release mechanism for NaDc is directly related to the medium pH, and the medium pH was very effective on the amount of release of the loaded drug. An important reality concluded from this data is that both AuNPs/p(AETAC-co-VI)/Q and p(AETAC-co-VI)/Q hydrogels released drugs held in the structure more rapidly as the medium pH increased. As the medium pH value increased, the release of drug molecules into the medium was eased as a result of deprotonation of the quaternized imidazole ring in the hydrogel network structure. In pH 8.0 (SWF) solution, the p(AETAC-co-VI)/Q hydrogel released nearly 80% within 5 h, while the AuNPs/p(AETAC-co-VI)/Q nanocomposite hydrogel released nearly 50% in 5 h. The release duration of NaDc in buffer solution from AuNPs/p(AETAC-co-VI)/Q is different because the presence of gold nanoparticles makes drug migration more difficult compared to p(AETAC-co-VI)/Q [54]. Additionally, the AuNPs/p(AETAC-co-VI)/Q hydrogel had higher loading capacity, as it displayed more drug release.

The Korsmeyer–Peppas model was applied to determine the mechanism of NaDc release and kinetic release parameters for p(AETAC-co-VI)/Q hydrogel and AuNPs/p(AETAC-co-VI)/Q nanocomposite, and the results are listed in Table 3. The slope and intersection points on the graphs in Fig. 10c and d were used to calculate the diffusion exponent and characteristic constant values for both situations. The value calculated for diffusion exponent revealed that the diffusion type in all release media was non-Fickian for both p(AETAC-co-VI)/Q and AuNPs/p(AETAC-co-VI)/Q. Accordingly, the drug release mechanism is controlled by diffusion and loosening of the polymer chain [55].

Conclusion

The main purpose of this study was to prepare AuNPs/p(AETAC-co-VI)/Q nanocomposite and p(AETAC-co-VI)/Q hydrogels as wound dressing material using the free radical polymerization technique, which is a simple and fast synthesis method, and examine their use for continuous release of the non-steroidal anti-inflammatory sodium diclofenac (NaDc) model drug. The structure and morphology of p(AETAC-co-VI)/Q hydrogels were examined by FTIR and SEM, respectively. XRD and TEM confirmed that gold nanoparticles were included in the p(AETAC-co-VI)/Q hydrogel matrix. In addition to characterization studies, swelling capabilities in distilled water, pH 6.0 (PB), pH 7.2 (PBS), and pH 8.0 (SWF) buffer solutions were investigated and found to reach swelling equilibrium within 7 h. A lower ratio of swelling was exhibited in the SWF medium because deprotonation of the protonated VI ring occurs in the simulated intestinal fluid. It was observed that p(AETAC-co-VI)/Q hydrogels follow the non-Fickian diffusion mechanism in all media. As the pH increased, the swelling value decreased, this is due to the deprotonation of the VI ring of the p(AETAC-co-VI)/Q hydrogels. Hydrogels with gold ion nanospheres showed activity against *E. coli* and *S. aureus*. The drug loading mechanism between AuNPs/p(AETAC-co-VI)/Q nanocomposite hydrogels and NaDc occurred through electrostatic interaction. NaDc release was gradual in pH 6.0 (PB), pH 7.2 (PBS), and pH 8.0 (SWF) media and showed a 93% continuous and controlled drug release behavior for 12 h in SWF medium. In the simulated wound fluid, deprotonation of VI groups occurs, and the drug molecules detach from the AuNPs/p(AETAC-co-VI)/Q nanocomposite hydrogels, resulting in faster release. In addition, the release mechanism from AuNPs/p(AETAC-co-VI)/Q nanocomposite hydrogels was observed to follow the non-Fickian diffusion mechanism. AuNPs/p(AETAC-co-VI)/Q nanocomposite hydrogels have a double effect on drug release and bacterial control of nanocomposite hydrogels. Therefore, considering sodium diclofenac as a model drug, low-cost nontoxic AuNPs/p(AETAC-co-VI)/Q nanocomposite hydrogels can be used as promising drug delivery systems.

Acknowledgements This work was financially supported by Çanakkale Onsekiz Mart University Scientific Research Coordination Unit (project number: FBA-2020-3231).

Declaration

Conflict of interest The authors declare no competing interests.

References

1. Aswathy SH, Narendrakumar U, Manjubala I (2020) Commercial hydrogels for biomedical applications. Heliyon 6:e03719. https://doi.org/10.1016/j.heliyon.2020.e03719

2. Chen J, Peng Q, Peng X, Han L, Wang X, Wang J, Zeng H (2020) Recent advances in mechano-responsive hydrogels for biomedical applications. ACS Appl Polym Mater 2:1092–1107. https://doi.org/10.1021/acsapm.0c00019
3. Mantha S, Pillai S, Khayambashi P, Upadhyay A, Zhang Y, Tao O, Pham HM, Tran SD (2019) Smart hydrogels in tissue engineering and regenerative medicine. Materials (Basel) 12(20):3323. https://doi.org/10.3390/ma12203323
4. Rezvani Ghomi E, Khalili S, Nouri Khorasani S, Esmaeely Neisiany R, Ramakrishna S (2019) Wound dressings: current advances and future directions. J Appl Polym Sci 136(27):47738. https://doi.org/10.1002/app.47738
5. Cascone S, Lamberti G (2020) Hydrogel-based commercial products for biomedical applications: a review. Int J Pharm 573:118803. https://doi.org/10.1016/j.ijpharm.2019.118803
6. Xiang J, Shen L, Hong Y (2020) Status and future scope of hydrogels in wound healing: synthesis, materials and evaluation. Eur Polym J 130:109609. https://doi.org/10.1016/j.eurpolymj.2020.109609
7. Muñoz-Bonilla A, Fernández-García M (2015) The roadmap of antimicrobial polymeric materials in macromolecular nanotechnology. Eur Polym J 65:46–62. https://doi.org/10.1016/j.eurpolymj.2015.01.030
8. Gupta A, Kowalczuk M, Heaselgrave W, Britland ST, Martin C, Radecka I (2019) The production and application of hydrogels for wound management: a review. Eur Polym J 111:134–151. https://doi.org/10.1016/j.eurpolymj.2018.12.019
9. Zhang L, Yin H, Lei X, Lau JNY, Yuan M, Wang X, Zhang F, Zhou F, Qi S, Shu B, Wu J (2019) A systematic review and meta-analysis of clinical effectiveness and safety of hydrogel dressings in the management of skin wounds. Front Bioeng Biotechnol 7(342):1–16. https://doi.org/10.3389/fbioe.2019.00342
10. Zhu T, Mao J, Cheng Y, Liu H, Lv L, Ge M, Li S, Huang J, Chen Z, Li H, Yang L, Lai Y (2019) Recent progress of polysaccharide-based hydrogel interfaces for wound healing and tissue engineering. Adv Mater Interfaces 6(17):1900761. https://doi.org/10.1002/admi.201900761
11. Li S, Dong S, Xu W, Tu S, Yan L, Zhao C, Ding J, Chen X (2018) Antibacterial hydrogels. Adv Sci (Weinh) 5(5):1700527. https://doi.org/10.1002/advs.201700527
12. Bhowmick S, Mohanty S, Koul V (2016) Fabrication of transparent quaternized PVA/silver nanocomposite hydrogel and its evaluation as an antimicrobial patch for wound care systems. J Mater Sci Mater Med 27:160. https://doi.org/10.1007/s10856-016-5772-8
13. Xue Y, Xiao H, Zhang Y (2015) Antimicrobial polymeric materials with quaternary ammonium and phosphonium salts. Int J Mol Sci 16(12):3626–3655. https://doi.org/10.3390/ijms16023626
14. Druvari D, Koromilas N, Bekiari V, Bokias G, Kallitsis J (2018) Polymeric antimicrobial coatings based on quaternary ammonium compounds. Coatings 8(1):8. https://doi.org/10.3390/coatings8010008
15. Wang K, Wang J, Li L, Xu L, Feng N, Wang Y, Fei X, Tian J, Li Y (2019) Synthesis of a novel anti-freezing, non-drying antibacterial hydrogel dressing by one-pot method. Chem Eng J 372:216–225. https://doi.org/10.1016/j.cej.2019.04.107
16. Caillier L, de Givenchy ET, Levy R, Vandenberghe Y, Géribaldi S, Guittard F (2009) Synthesis and antimicrobial properties of polymerizable quaternary ammoniums. Eur J Med Chem 44(8):3201–3208. https://doi.org/10.1016/j.ejmech.2009.03.031
17. Xu C, Akakuru OU, Ma X, Zheng J, Zheng J, Wu A (2020) Nanoparticle-based wound dressing: recent progress in the detection and therapy of bacterial infections. Bioconjug Chem 31(7):1708–1723. https://doi.org/10.1021/acs.bioconjchem.0c00297
18. Bhowmick S, Koul V (2016) Assessment of PVA/silver nanocomposite hydrogel patch as antimicrobial dressing scaffold: synthesis, characterization and biological evaluation. Mater Sci Eng C Mater Biol Appl 59:109–119. https://doi.org/10.1016/j.msec.2015.10.003
19. Dykman LA, Khlebtsov NG (2011) Gold nanoparticles in biology and medicine: recent advances and prospects. Acta Nat 3(2):34–55. https://doi.org/10.32607/20758251-2011-3-2-34-55
20. Singh J, Kumar S, Dhaliwal AS (2020) Controlled release of amoxicillin and antioxidant potential of gold nanoparticles-xanthan gum/poly (acrylic acid) biodegradable nanocomposite. J Drug Deliv Sci Tec 55:101384. https://doi.org/10.1016/j.jddst.2019.101384
21. Hashmi ASK, Hutchings GJ (2006) Gold catalysis. Angew Chem Int Ed 45:7896–7936. https://doi.org/10.1002/anie.200602454
22. Hendrich CM, Sekine K, Koshikawa T, Tanaka K, Hashmi ASK (2020) Homogeneous and heterogeneous gold catalysis for materials science. Chem Rev. https://doi.org/10.1021/acs.chemrev.0c00824
23. Nasef SM, Khozemy EE, Mahmoud GA (2019) Characterization and in vitro drug release properties of chitosan/acrylamide/gold nanocomposite prepared by gamma irradiation. Int J Polym Mater Po 68:723–732. https://doi.org/10.1080/00914037.2018.1493685
24. Grzelczak M, Pérez-Juste J, Mulvaney P, Liz-Marzán LM (2008) Shape control in gold nanoparticle synthesis. Chem Soc Rev 37(8):1783–1791. https://doi.org/10.1039/b711490g
25. Katas H, Lim CS, Nor Azlan AYH, Buang F, Mh Busra MF (2019) Antibacterial activity of biosynthesized gold nanoparticles using biomolecules from Lignosus rhinocerotis and chitosan. Saudi Pharm J 27(2):283–292. https://doi.org/10.1016/j.jsps.2018.11.010
26. Folorunso A, Akintelu S, Oyebamiji AK, Ajayi S, Abiola B, Abdusalam I, Morakinyo A (2019) Biosynthesis, characterization and antimicrobial activity of gold nanoparticles from leaf extracts of Annona muricata. J Nanostruct Chem 9:111–117. https://doi.org/10.1007/s40097-019-0301-1
27. Lin S, Jiang S, Zhang Y, Dai Z, Dai Y, Xia F, Zhang X (2021) Gold nanorods crosslinking PNIPAM hydrogels via dynamic Au-thiolate interaction with stretchable, adhesive, self-healing, and photothermal properties. Gold Bull 54:59–67. https://doi.org/10.1007/s13404-021-00293-6
28. Mordorski B, Prow T (2016) Nanomaterials for wound healing. Curr Derm Rep 5:278–286. https://doi.org/10.1007/s13671-016-0159-0
29. Kavetskyy T, Stasyuk N, Smutok O, Demkiv O, Kukhazh Y, Hoivanovych N, Boev V, Ilcheva V, Petkova T, Gonchar M (2019) Improvement of amperometric laccase biosensor using enzyme-immobilized gold nanoparticles coupling with ureasil polymer as a host matrix. Gold Bull 52:79–85. https://doi.org/10.1007/s13404-019-00255-z
30. Ma K, Cheng Y, Wei X, Chen D, Zhao X, Jia P (2020) Gold embedded chitosan nanoparticles with cell membrane mimetic polymer coating for pH-sensitive controlled drug release and cellular fluorescence imaging. J Biomater Appl 10:1–12. https://doi.org/10.1177/0885328220952594
31. Zhu S, Wang X, Liu L, Li L (2020) Gold nanocluster grafted conjugated polymer nanoparticles for cancer cell imaging and photothermal killing. Colloid Surf A 597:124764. https://doi.org/10.1016/j.colsurfa.2020.124764
32. Marsich E, Travan A, Donati I, Di Luca A, Benincasa M, Crosera M, Paoletti S (2011) Biological response of hydrogels embedding gold nanoparticles. Colloid Surface B 83(2):331–339. https://doi.org/10.1016/j.colsurfb.2010.12.002
33. Im P, Kim J (2018) On-demand macroscale delivery system based on a macroporous cryogel with a high drug loading capacity for enhanced cancer therapy. ACS Biomater Sci Eng 4(10):3498–3505. https://doi.org/10.1021/acsbiomaterials.8b00911
34. Kurdtabar M, Baghestani G, Bardajee GR (2019) Development of a novel thermo-responsive hydrogel-coated gold nanorods as a drug delivery system. Gold Bull 52(1):9–17. https://doi.org/10.1007/s13404-018-0248-x

35. Sadat Akhavi S, Moradi Dehaghi S (2020) Drug delivery of amphotericin B through core-shell composite based on PLGA/Ag/Fe3O4: In Vitro Test. Appl Biochem Biotechnol 191: 496–510. https://doi.org/10.1007/s12010-019-03181-0
36. Singh B, Dhiman A (2016) Design of acacia gum–carbopol–cross-linked-polyvinylimidazole hydrogel wound dressings for antibiotic/anesthetic drug Delivery. Ind Eng Chem Res 55(34):9176–9188. https://doi.org/10.1021/acs.iecr.6b01963
37. Onder A, Ilgin P, Ozay H, Ozay O (2020) Removal of dye from aqueous medium with pH-sensitive poly[(2-(acryloyloxy)ethyl)trimethylammonium chloride-co-1-vinyl-2-pyrrolidone] cationic hydrogel. J Environ Chem Eng 8(5):104436. https://doi.org/10.1016/j.jece.2020.104436
38. Kıvanç MR, Ozay O, Ozay H, Ilgin P (2020) Removal of anionic dyes from aqueous media by using a novel high positively charged hydrogel with high capacity. J Dispers Sci Technol:1–16. https://doi.org/10.1080/01932691.2020.1847658
39. Ilgin P, Ozay H, Ozay O (2020) Synthesis and characterization of pH responsive alginate based-hydrogels as oral drug delivery carrier. J Polym Res 27:251. https://doi.org/10.1007/s10965-020-02231-0
40. Ozay H, Ilgin P, Ozay O (2019) Novel hydrogels based on crosslinked chitosan with formyl-phosphazene using Schiff-base reaction. Int J Polym Mater Polym Biomater:1–10. https://doi.org/10.1080/00914037.2019.1706514
41. Ilgin P, Ozay H, Ozay O (2019) A new dual stimuli responsive hydrogel: modeling approaches for the prediction of drug loading and release profile. Eur Polym J 113:244–253. https://doi.org/10.1016/j.eurpolymj.2019.02.003
42. Siepmann J, Peppas NA (2001) Modeling of drug release from delivery systems based on hydroxypropyl methylcellulose (HPMC). Adv Drug Deliv Rev 48(2-3):139–157. https://doi.org/10.1016/S0169-409X(01)00112-0
43. Pekel N, Güven O (2002) Synthesis and characterization of poly(N-vinyl imidazole) hydrogels crosslinked by gamma irradiation. Polym Int 51(12):1404–1410. https://doi.org/10.1002/pi.1065
44. Genç F, Uzun C, Güven O (2016) Quaternized poly(1-vinylimidazole) hydrogel for anion adsorption. Polym Bull 73: 179–190. https://doi.org/10.1007/s00289-015-1479-0
45. Heidari S, Esmaeilzadeh F, Mowla D, Ghasemi S (2018) Synthesis of an efficient copolymer of acrylamide and acrylic acid and determination of its swelling behavior. J Pet Explor Prod Technol 8: 1331–1340. https://doi.org/10.1007/s13202-017-0428-x
46. Horkay F, Tasaki I, Basser PJ (2000) Osmotic swelling of polyacrylate hydrogels in physiological salt solutions. Biomacromolecules 1(1):84–90. https://doi.org/10.1021/bm9905031
47. Primo GA, Garcia Manzano MF, Romero MR, Alvarez Igarzabal CI (2015) Synthesis and characterization of hydrogels from 1-vinylimidazole. Highly resistant co-polymers with synergistic effect. Mater Chem Phys 153:365–375. https://doi.org/10.1016/j.matchemphys.2015.01.027
48. Veerakumar P, Sangili A, Chen S-M, Lin K-C (2020) Ultrafine gold nanoparticle embedded poly(diallyldimethylammonium chloride)–graphene oxide hydrogels for voltammetric determination of an antimicrobial drug (metronidazole). J Mater Chem C 8:7575–7590. https://doi.org/10.1039/C9TC06690J
49. Tepale N, Fernández-Escamilla VVA, Carreon-Alvarez C, González-Coronel VJ, Luna-Flores A, Carreon-Alvarez A, Aguilar J (2019) Nanoengineering of gold nanoparticles: green synthesis, characterization, and applications. Crystals 9(12):612. https://doi.org/10.3390/cryst9120612
50. Bardajee GR, Mizani F, Hosseini SS (2017) pH sensitive release of doxorubicin anticancer drug from gold nanocomposite hydrogel based on poly(acrylic acid) grafted onto salep biopolymer. J Polym Res 24:4. https://doi.org/10.1007/s10965-017-1197-4
51. Ozay H, Tarımeri N, Gungor Z, Demirbakan B, Özcan B, Sezgintürk MK, Ozay O (2020) A new approach to synthesis of highly dispersed gold nanoparticles via glucose oxidase-immobilized hydrogel and usage in the reduction of 4-nitrophenol. ChemistrySelect 5(29):9143–9152. https://doi.org/10.1002/slct.202002327
52. Mandal B, Rameshbabu AP, Dhara S, Pal S (2017) Nanocomposite hydrogel derived from poly (methacrylic acid)/carboxymethyl cellulose/AuNPs: a potential transdermal drugs carrier. Polymer 120: 9–19. https://doi.org/10.1016/j.polymer.2017.05.042
53. Prusty K, Swain SK (2019) Release of ciprofloxacin drugs by nano gold embedded cellulose grafted polyacrylamide hybrid nanocomposite hydrogels. Int J Biol Macromol 126:765–775. https://doi.org/10.1016/j.ijbiomac.2018.12.258
54. Pereira AKDS, Reis DT, Barbosa KM, Scheidt GN, da Costa LS, Santos LSS (2020) Antibacterial effects and ibuprofen release potential using chitosan microspheres loaded with silver nanoparticles. Carbohydr Res 488:107891. https://doi.org/10.1016/j.carres.2019.107891
55. Ozay H, Ilgin P, Ozyurt C, Ozay O (2020) The single-step synthesis of thiol-functionalized phosphazene-based polymeric microspheres as drug carrier. Polymer-Plastics Technol Mater 59(17):1944–1955. https://doi.org/10.1080/25740881.2020.1784212